Langmuir
Article
pubs.acs.org/Langmuir

Dynamic Behaviors of Droplet Impact and Spreading: Water on Five Different Substrates

Meng-Jiy Wang, Fang-Hsing Lin, Yi-Lin Hung, and Shi-Yow Lin*

Department of Chemical Engineering, National Taiwan University of Science and Technology, 43, Keelung Rd., Sec. 4, Taipei 106, Taiwan

Received January 23, 2009. Revised Manuscript Received March 9, 2009

The dynamic wetting behaviors, especially the droplet morphology, of a water droplet impinging on five substrate surfaces were investigated. A water drop was released from 13.6 mm above a solid surface and impinged on substrates. The images (the silhouette and 45° top view) were sequentially recorded from the moment that the droplet impacted the solid surface until it reached equilibrium. The entire profile of each of the water droplets during spreading was obtained from the digitized recorded images. The digitized droplets were then used to detail the spreading mechanism, including information on the relaxations of the wetting diameter, droplet height, contact angle, and spreading velocity. A comparison of the full droplet profiles allows us to clarify the independent motion of two related but independent components, the central region and rim, of an impinging droplet. An interesting plateau region in the droplet height relaxation curve was observed in the first cycle for all substrate surfaces. For hydrophobic surfaces (paraffin and Teflon), three particular growth modes in the droplet height relaxation curve were detected in every oscillation cycle during the early spreading stages. It only took three and four oscillation cycles for a water droplet on the glass and quartz substrates, respectively, to dissipate its energy and reach its equilibrium state. However, it took 72 and 28 oscillation cycles for a water droplet on the Teflon and paraffin substrates, respectively. Moreover, several other new phenomena were also observed.

Introduction

The droplet impact phenomenon appears ubiquitously in daily life in areas ranging from coffee splitting, standing in the shower, early morning dew, and self-cleaning of leaves. The importance of this phenomenon has been addressed for over a century due to the special physical processes involved. The extensive industrial applications of droplet impaction include agriculture, printing, and adhesion.[1−3]

Droplet impingement on solid substrates is a complex process that encompasses aspects of fluid dynamics, physics, and interfacial chemistry. Research on droplet impaction has been studied theoretically, numerically, and experimentally. For example, the critical conditions for the occurrences of detachment, splashing, and/or rebound can be determined both numerically and experimentally.[4,5] The correlations between the maximum spreading diameter, spreading rate, and droplet retraction have been extensively investigated.[6−8] Experimental data on spreading and retraction have also been compared with theoretical predictions by considering the energy balance of liquid−solid interactions.[9−13]

The major factors affecting droplet impact behavior are the droplet properties and liquid−solid interaction. The droplet properties include impact velocity, drop size, liquid viscosity, and surface tension. They are usually described as dimensionless parameters (Reynolds, Weber, and Ohnesorge numbers).[14,15] The Weber number relates inertia and surface tension energies; therefore, it can be used to help identify the dominant parameters during the course of spreading.[16] It is noted that, at low *We* number, the impinging droplet spreads instantly over the surface with nearly no rebounding behavior. Splashing or rebounding may occur at high *We*. In this study, droplets of low *We* (*We* < 10) were applied to investigate the wetting and spreading behaviors with a low initial impact velocity.

Mao et al.[17] reported that a surface hydrophobicity of $\theta = 37°-97°$ has nearly no effect on the maximum spreading diameter (d_{max}) at low *We* for water droplets of millimeter size. However, Dong et al.[18] concluded that d_{max} depends strongly on the surface hydrophobicity of substrates (at $\theta = 6°-107°$) for 40 μm water droplets with *We* = 2.7−103. In addition to the maximum spreading diameter, ring formation and the spreading factor have been found to be surface hydrophobicity dependent.[4,19,20]

There are more parameters, such as roughness, hardness, and surface energy of substrates, which will also affect drop impingement behaviors significantly.[21] Some parameters affecting the

*To whom correspondence should be addressed: Tel +886-2-2737-6648, Fax +886-2-2737-6644, e-mail sylin@mail.ntust.edu.tw.

(1) Worthington, A. M. *Proc. R. Soc. London* **1877**, *25*, 261–272.
(2) Rein, M. *Fluid Dyn. Res.* **1993**, *12*, 61–93.
(3) Yi, U.; Kim, C. *Sens. Actuators, A* **2004**, *114*, 347–354.
(4) Fukai, J.; Shiiba, Y.; Yamamoto, T.; Miyatake, O.; Poulikakos, D.; Megaridis, C. M.; Zhao, Z. *Phys. Fluids* **1995**, *7*, 236–247.
(5) Renardy, Y.; Popinet, S.; Duchemin, L.; Renardy, M.; Zaleski, S.; Josserand, C.; Drumright-Clarke, M.-A.; Richard, D.; Clanet, C.; Quere, D. *J. Fluid Mech.* **2003**, *484*, 69–83.
(6) Dodge, F. T. *J. Colloid Interface Sci.* **1988**, *121*, 154–160.
(7) Galvin, K. P.; Cork, A.; Wall, T. F. *Colloids Surf., A* **1996**, *113*, 107–116.
(8) Healy, W. M.; Hartley, J. G.; Abdel-Khalik, S. I. *Int. J. Heat Mass Transfer* **2001**, *44*, 235–240.
(9) Blake, T. D.; Ruschak, K. J. *Nature (London)* **1979**, *282*, 489–491.
(10) Blake, T. D.; Clarke, A.; Ruschak, K. J. *AIChE J.* **1994**, *40*, 229–242.
(11) Blake, T.; Clarke, A.; Coninck, J. D.; Ruijter, M. D. *Langmuir* **1997**, *13*, 2164–2166.
(12) Berim, G. O.; Ruckenstein, E. *J. Phys. Chem. B* **2004**, *108*, 19330–19338.
(13) Attane, P.; Girard, F.; Morin, V. *Phys. Fluids* **2007**, *19*, 012101.
(14) Schiaffino, S.; Sonin, A. A. *Phys. Fluids* **1997**, *9*, 3172–3187.
(15) Crooks, R. C.; Cooper-White, J. J.; Boger, D. V. *Chem. Eng. Sci.* **2001**, *56*, 5575–5592.
(16) Ge, Y.; Fan, L. S. *Phys. Fluids* **2005**, *17*, 027104.
(17) Mao, T.; Kuhn, D. C. S.; Tran, H. *AIChE J.* **1997**, *43*, 2169–2179.
(18) Dong, H.; Carr, W. W.; Bucknall, D. G.; Morris, J. F. *AIChE J.* **2007**, *53*, 2606–2617.
(19) Šikalo, Š.; Marengo, M.; Tropea, C.; Ganic, E. N. *Exp. Therm. Fluid Sci.* **2002**, *25*, 503–510.
(20) Šikalo, S.; Tropea, C.; Ganic, E. N. *Exp. Therm. Fluid Sci.* **2005**, *29*, 798–802.
(21) Ukiwe, C.; Kwok, D. Y. *Langmuir* **2005**, *21*, 666–673.

environment, such as magnetic or electric fields, are also important on the investigations of impinging droplets.[22−26]

In this study, one of the key parameters, surface hydrophobicity, is investigated by impinging water droplets on five different substrates (with θ = 9.5°−111°) at fixed *We* and *Re* (Reynolds) numbers. By fixing the droplet diameter (*d*) and impact velocity for all experimental runs, both *Re* and *We* were kept constant. Beside, all measurements were performed at low *We* number by using a small droplet height. The advantage of using a low *We* is the ability to observe the wetting behavior clearly and thus provide the necessary data for quantitative analyses. Some interesting phenomena were observed. For example, a novel plateau region in the course of droplet height (*h*) relaxation was identified on all five substrates during the initial spreading. On hydrophobic surfaces, three particular growth modes in *h* evolution were detected during the droplet ascending and descending courses.

Quantitative analyses were facilitated by plotting the sequential images taken using a high-speed camera together with the sequential full droplet profiles. The effects of surface hydrophobicity on wetting behaviors were examined in detail by monitoring the relaxations in the wetting diameter, droplet height, and contact angle. Other data, including the spreading rate, oscillation behaviors, oscillation period, oscillation amplitude, and the time required to reach equilibrium, are also reported.

Experimental Section

Apparatus. High-speed video-enhanced image digitization equipment (Figure 1) was used to create a silhouette and an image from a 45° or 58° top view of an impinging droplet to video-image the silhouette and to digitize the image.[27] The apparatus consisted of a halogen light source (10 W, only 3% of the light passes through the filter), a plano-convex lens system for producing a collimated beam, an objective lens (effective focal length 96 mm), and a solid-state camera (CA-D1, DALSA). Falling drops were generated from a stainless steel needle (gauge no. 31, i.d. = 0.13 mm and o.d. = 0.26 mm), which was *h* mm above the solid substrate (h = 13.6 ± 0.2 mm, the distance between the solid surface and the bottom of the pendant drop). A video-image digitizer (Oculus F/64) digitized the pictures into 64 lines × 64 pixels, each of which was assigned a gray level value with an 8-bit resolution. The rate of image acquisition was 2905 images/s. The system was capable of acquiring 4100 sequential images. The temperature change of a sessile drop in this apparatus was undetectable (< 0.1 °C) in 200 s. Note that the experiment was done in a few seconds.

An edge detection routine was devised in the following way. The change in the gray level ranged from the black (0) inside to the bright light (255) outside in a few pixels. The change was not a stepwise increase from 0 to 255 but was gradual. The variation was nearly symmetric around 127.5, and the edge was defined at the position with a 127.5 gray level. The change was almost linear around a gray level of 127.5. Therefore, the edge was defined as the *x* or *y* position that, for the interpolated line, corresponded to an intensity of 127.5. The uncertainty for the edge location was ∼0.1 pixels. The image forming system was calibrated by digitizing a stainless steel ball with a known diameter of 2.498 ± 0.002 mm. The coordinates of the digitized sphere were processed to calibrate the average length between pixels along a row and along a column. The calibration procedure yielded values of 114.4 μm/pixel horizontally and 116.0 μm/pixel vertically.

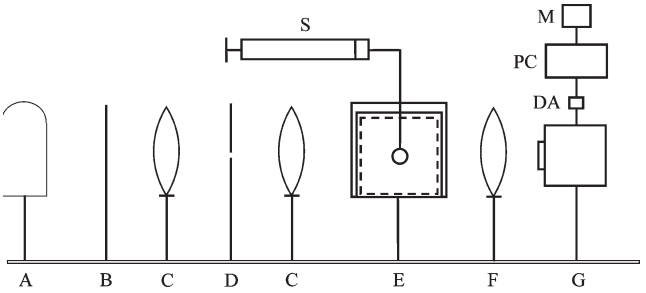

Figure 1. Video-enhanced impinging droplet image digitization system: A = light source, B = filter, C = biconvex lens, D = pinhole, DA = D/A data translation card, E = chamber and suspending needle, F = objective lens, G = CCD camera, M = monitor, PC = personal computer, S = syringe.

Free-Falling Drop. After detaching from the needle tip, a drop would follow a free-falling body movement as it fell. The droplet was monitored for a range of 6 mm height before contacting the substrate. A deformation (oscillation) of droplet was observed before the impact. The variations of vertical (D_v) and horizontal (D_h) diameters of the falling droplet were ∼5% of its diameter. Two common average diameters, $D_1 = (D_h^2 D_v)^{1/3}$ and $D_2 = (D_h D_v)^{1/2}$, were calculated and compared. A smaller variation is obtained using $(D_h D_v)^{1/2}$. The average diameter, $D_{2,avg} = [\sum_i^N D_2(t_i)]/N$, during the monitored 6 mm range was assigned to be the droplet diameter.

Materials and Methods. The impinging water droplet was purified by a Millipore water purification system, and the output water had a specific conductance of 0.056 μS/cm. Microscope glass, quartz, Teflon (from Dinhaw Co., Taiwan), and paraffin (Parafilm M film, from Pechiney plastic packaging) were used as the solid substrates. The paraffin was evenly stretched a little bit and covered on a microscope glass. The film is well attached on the glass. The horizontal positions of solid surfaces were carefully checked before the droplet impinging experiments.

The cleaning procedure for the glass and quartz was as follows: glass and quartz were immersed in cleaning solution (strong acid) for ca. 2 h, after which they were rinsed with a large volume of pure water and then immersed in a diluted HCl solution. Immediately before measurement, the glass and quartz were rinsed with pure water. The glass substrate cleaned by this procedure is referred to as "clean glass" henceforth.

The second glass substrate (referred to as "glass-2" in the subsequent text) was microscope glass that was rinsed with pure water 20 times before measurement, without using a cleaning solution. The Teflon was cleaned by an ultrasonic bath cleaner and then rinsed several times using dilute methanol and pure water before use. Parafilm M film was used as received.

A droplet was generated at the tip of a needle which was 13.6 ± 0.2 mm above the solid substrate so it would have an impact velocity 517 ± 4 mm/s. The droplet fell and impinged upon the solid substrate. Sequential digital images of the drop were then taken, first at intervals of 1/2905 s for 1.2 s and then in intervals of 1/100 s for around 5 s. All experiments were undertaken at 25 ± 0.5 °C. After the impinging action was completed, the images were processed to determine the drop edge coordinates, the full profile of the impinging droplets, droplet height, and the diameter of the three-phase contact circle.

The surface morphology of the clean glass and glass-2 were analyzed by a Digital Instruments Nanoscope III atomic force microscope (AFM, Veeco Ltd.). The tapping mode was employed for the scanning. In addition, the surface carbon contents of the clean glass and glass-2 were identified by recording the ESCA spectra (electron spectroscopy for chemical analysis) on a Thermo VG Scientific Theta Probe Instrument using Al (1486.6 eV) and Mg (1253.6 eV) as excitation sources. Data processing including

(22) Blake, T. D.; Coninck, J. D. *Adv. Colloid Interface Sci.* **2002**, *96*, 21–36.
(23) Lee, J.; Kim, C. *J. Microelectromech. Syst.* **2000**, *9*, 171–180.
(24) Zhang, X.; Basaran, O. A. *J. Colloid Interface Sci.* **1997**, *187*, 166–178.
(25) Imano, A. M.; Beroual, A. *J. Colloid Interface Sci.* **2006**, *298*, 869–879.
(26) Werner, S. R.; Jones, J. R.; Paterson, A. H.; Archer, R. H.; Pearce, D. L. *Chem. Eng. Sci.* **2007**, *62*, 2336–2345.
(27) Lin, S. Y.; McKeigue, K.; Maldarelli, C. *AIChE J.* **1990**, *36*, 1785–1795.

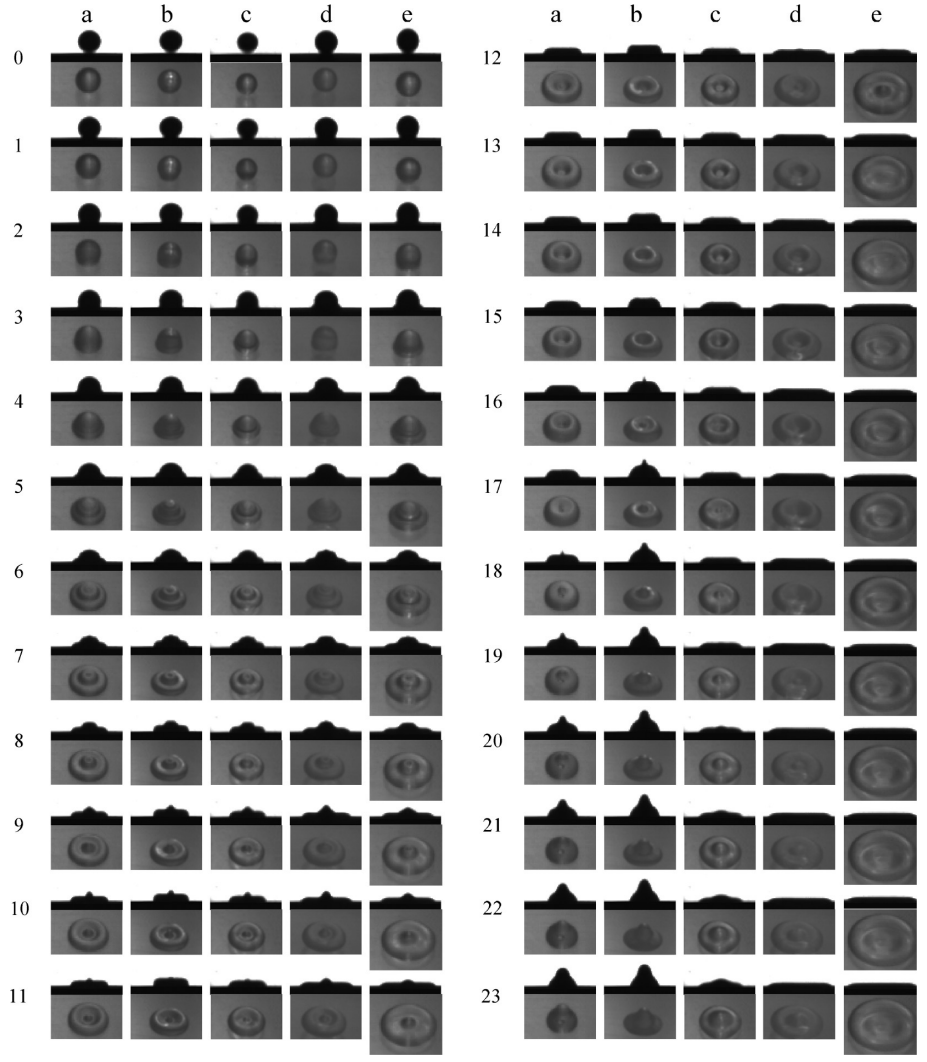

Figure 2. Illustration of the wetting behavior of impinging droplets onto paraffin (a), Teflon (b), glass-2 (c), quartz (d), and clean glass (e) surfaces, showing the silhouettes and images from 45° (b, c, d) or 58° (a, e) top view. The number on the left-hand side represents the sequence of images after impact. The exact impact time of $t = 0$ is located between image nos. 0 and 1. The time interval between two images is 1/2905 s.

background subtraction and integration was carried out using the Peak-fit software.

Images were recorded of the drop before impact. The positions of the top and bottom points were fit by the free-falling body equation to determine the time of droplet contact and the impact velocity. The difference between the contact times estimated from the top and bottom points was usually around 0.1−0.2 image numbers (1 image number = 1/2905 s). This disagreement was resulted from the oscillation of the falling droplet in air.

Results

A water droplet was released from the tip of a needle (gauge #31) in which the bottom of the pendant droplet was 13.6 ± 0.2 mm above the solid substrate. Thus, droplets with constant diameter (2.14 ± 0.03 mm) and impact velocity (517 ± 4 mm/s) were generated. Therefore, all the water droplets used in this study had the same Reynolds (1104 ± 15) and Weber (7.9 ± 0.1) numbers. The images were recorded sequentially (the silhouette and 45° or 58° top view) starting from immediately before the moment when the droplet impacted the solid surface until it reached equilibrium. Figure 2 shows the first 23 images following impact. The full profiles of the water droplets during spreading were generated from the digitized images, as shown in Figure 3. The digitized droplets were able to provide a clear view of the spreading mechanism: the relaxations of wetting diameter, of droplet height, of contact angle, and of spreading velocity.

In order to investigate the dynamic behavior of droplet impaction, five different solid substrates (paraffin, Teflon, glass-2, quartz, and clean glass) were utilized. The advancing contact angles of the water droplet for each surface are listed in Table 1. The effects of the hydrophobicity of solid surfaces on the dynamic droplet height, wetting diameter, and contact angle were examined.

1. Short-Term Phenomenon. *Plateau Behavior*. When the droplet impacted the surface, it spread rapidly and generated a shoulder region (Figures 2 and 3), which wet the solid surface and advanced horizontally. Moreover, the contact angle and droplet height decreased dramatically (Figure 4). The spreading then continued, and the shoulder extended and became a rimlike region. The contact angle (θ) decreased rapidly and leveled off in 2−4 image numbers (Figure 4b). Because of the fixed initial velocity in this study, the decreasing rates of θ were roughly the same for the five different substrates (the slopes are roughly the same except the blue line) (Figure 4b). These data imply that the decreasing rate of θ at the initial stage of an impinging droplet is independent of the surface properties and is mainly dependent on the kinetic energy. The profile of the decrease of droplet height shows a similar trend for all substrates for the first seven images (Figure 4d).

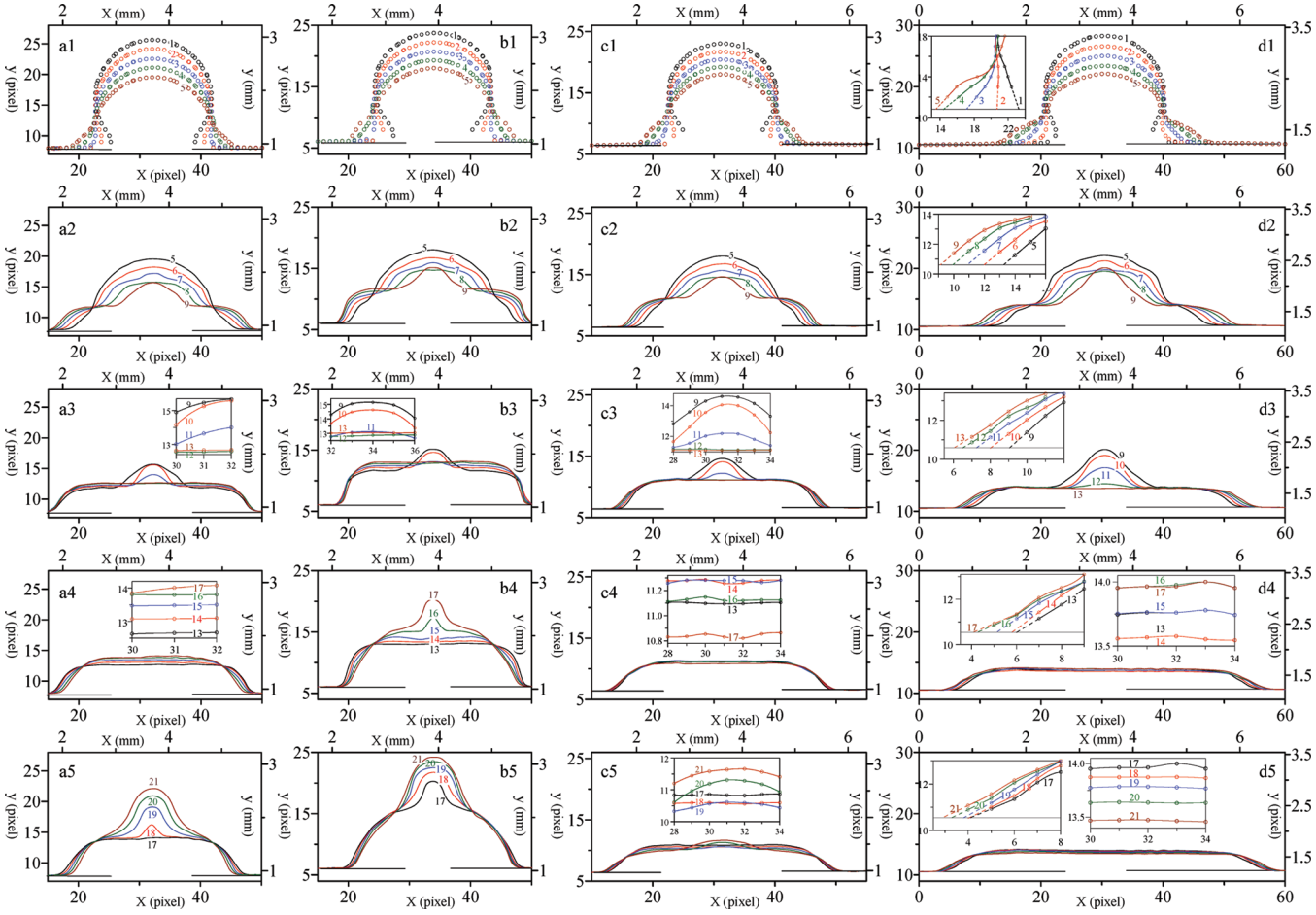

Figure 3. Illustrations of the dynamic droplet profiles for the spreading of droplets onto Teflon (a), paraffin (b), glass-2 (c), and quartz (d) surfaces. The number indicates the sequence of the images after droplet impact.

Table 1. Operation Conditions of Droplet Impingement

run	substrate	θ_a[f]	diameter (mm)	v[e] (mm/s)	*Re*	*We*	H[d] (mm)	cycle[c]	period[b] (image no.)	t_e[a] (image no.)
1	glass	9.5	2.15	524	1121	8.11	14.0	3	101	212
2	quartz	10	2.20	514	1121	7.95	13.5	4	74	234
3	glass-2	20	2.14	517	1103	7.92	13.6	5	40	192
4	Teflon	107	2.11	513	1088	7.79	13.4	72	26	1874
5	paraffin	111	2.12	517	1089	7.79	13.6	28	27	770

[a] Time to reach the equilibrium state (oscillation disappears). [b] Oscillation period of droplet height. [c] Oscillation cycle on droplet height before the oscillation disappears. [d] The height calculated from free-falling body equation based on the impact velocity. [e] Impact velocity. [f] Advancing contact angle.

At the end of this initial spreading stage, a significant plateau region appeared during the relaxation of drop height. This plateau formation is due to the change in shape of the central region from blunt to sharper. The central region retained a narrower conelike shape after this plateau region for a couple of images (Figure 3).

Diameter. Immediately after droplet impact, the spreading rate of droplet wetting was dependent on the hydrophobicity of the solid surface. The data in Figure 4f show that quartz and clean glass had a higher spreading rate than the other three substrates. In other words, the more hydrophobic the substrate is, the smaller the wetting rate. The droplet diameter for the extreme hydrophilic surfaces (clean glass and quartz) expanded faster and reached a larger d_{max}, but with only a small oscillation. The glass-2 had a moderate d_{max} with a moderate oscillation amplitude, and the hydrophobic surfaces (Teflon and paraffin) had a smaller d_{max} with a larger diameter oscillation (Figure 4e).

The droplet heights of the plateau (h_p) were different for different substrates (Figure 4d). The h_p was the lowest for clean glass, in the middle for glass-2 and paraffin, and the highest for Teflon and quartz. It was also noted that, for Teflon and quartz, the relaxation of droplet height demonstrated a slight overshooting behavior. This overshooting took place at the moment when the circular concave region began to form; therefore, the central cone was pushed upward slightly during this spreading.

The difference of droplet height at which the plateau occurred may be due to the effect of hardness and hydrophobicity. For surfaces with similar hydrophobicity, Teflon showed a higher h_p than paraffin because Teflon is much harder than paraffin. Similarly, the h_p for quartz was larger than that of clean glass due to the greater hardness of quartz. The hardness of clean glass is the same as that of glass-2, but glass-2 is more hydrophobic (Table 1). Therefore, glass-2 showed a higher h_p than clean glass.

If one carefully examines images 10−12 for Teflon, one can observe a complicated relationship between the droplet height, wetting diameter, and the height of the rim. First, the diameter of the rim (or the three-phase contact circle) reaches its maximum at ca. image 10 and then decreases with time. At this stage, the

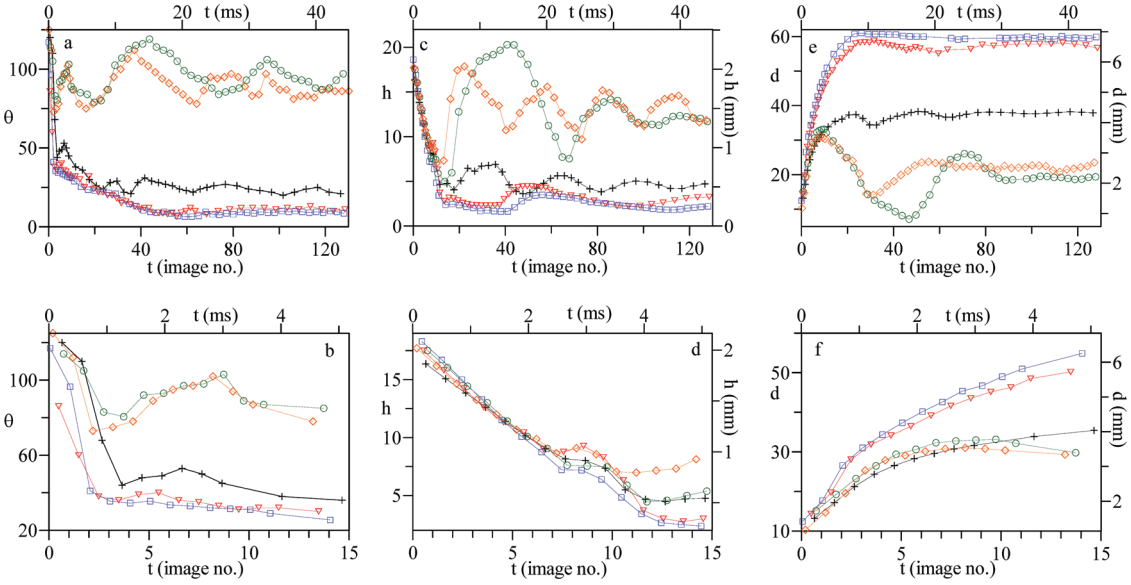

Figure 4. Relaxation of droplet wetting diameter (d), droplet height (h), and contact angle (θ) for water droplets impinging onto Teflon (◇), paraffin (○), glass-2 (+), quartz (▽), and clean glass (□) surfaces. Diameter and height are in pixels (= 114.4 μm) unit, and time (t) is measured by the image numbers (= 1/2905 s).

droplet height is decreasing also. In other words, during the time when the central conelike region (above the rim) decreases and then disappears, the droplet has started to retract. Note that the height of the rim increases during this stage. The decrease of the wetting diameter and the enlargement of the central concave region (columns a and b in Figure 2) after image 10 provide the height increase of the rim. Figure 5 illustrates the details of this phenomenon, which was observed for hydrophobic surfaces. No similar phenomenon was detected for hydrophilic surfaces (Figure 5c).

Oscillation. Table 1 shows the different aspects involved in the quantification of the oscillation behavior of droplet height: oscillation cycle, oscillation period, and the time to reach equilibrium. It only took three to four oscillation cycles, with a longer oscillation period, to reach equilibrium when the water droplet impinged on hydrophilic surfaces. The time needed to reach equilibrium (t_e: defined in this work as the time when the amplitude is less than 20 μm) for a water droplet on glass and quartz was much shorter than that on the hydrophobic surfaces. In addition, the period of oscillation depended strongly on the surface hydrophobicity; the surface with a smaller contact angle shows a larger oscillation period. For clean glass, quartz, and glass-2, the oscillation period was 101, 74, and 40 (image no.), respectively.

Compared with hydrophilic surfaces, the number of oscillations increased from 3 or 4 to 28 and 72 for paraffin and Teflon, respectively. The t_e for paraffin was 770 (image no.) and 1874 (image no.) for Teflon. Nearly the same t_e was observed for these two hydrophilic surfaces (around image no. 200).

2. Intermediate Time Period. *Wetting Diameter*. Droplet behaviors for images 15−80 are discussed below. The wetting diameter at an intermediate time period can be categorized into three groups. On clean-glass and quartz, the impinging droplet reached its maximum wetting diameter at about image no. 25 (Figure 6d,e), and the retraction and subsequent wetting behaviors were quite similar. For glass-2, the droplet reached a local maximum wetting at circa image no. 23, and d_{max} actually occurred after one more retraction and wetting cycle at image no. 54 (Figure 6c). Because of the different surface hydrophobicity, the d_{max} for glass-2 was only about 60% of clean-glass and

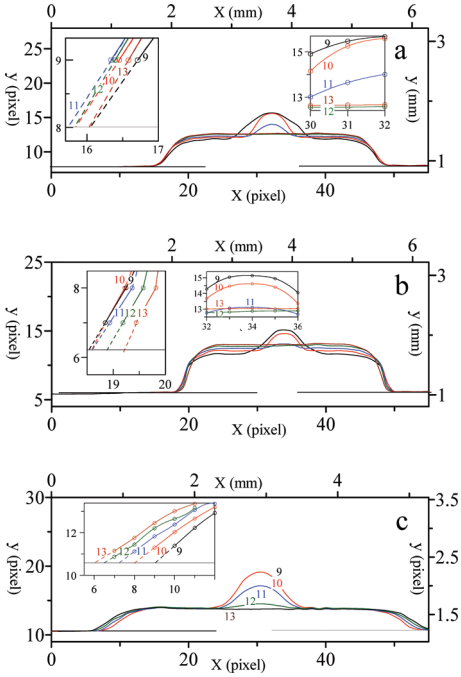

Figure 5. Illustrations of the dynamic droplet profiles for the spreading of droplets onto paraffin (a), Teflon (b), and quartz (c) surfaces, showing in more detail the partial motion of central and rim. The number indicates the sequence of the images after droplet impact.

quartz. Oscillation, retraction, and wetting for the impinging droplets occurred for all three hydrophilic surfaces. Figure 6c−e demonstrates clearly that the oscillation of wetting diameter for glass-2 was more significant than that for the other two hydrophilic surfaces.

For hydrophobic surfaces, the impinging droplet reached its d_{max} in a shorter time followed by a stronger retraction−wetting oscillation. However, the wetting diameter varied in a different manner for Teflon and paraffin (Figures 4e and 6a,b). The water droplet on paraffin retracted dramatically to a very small wetting diameter (7 pixels) and was followed by relatively strong wetting. In contrast, the droplet on the Teflon surface did not retract as

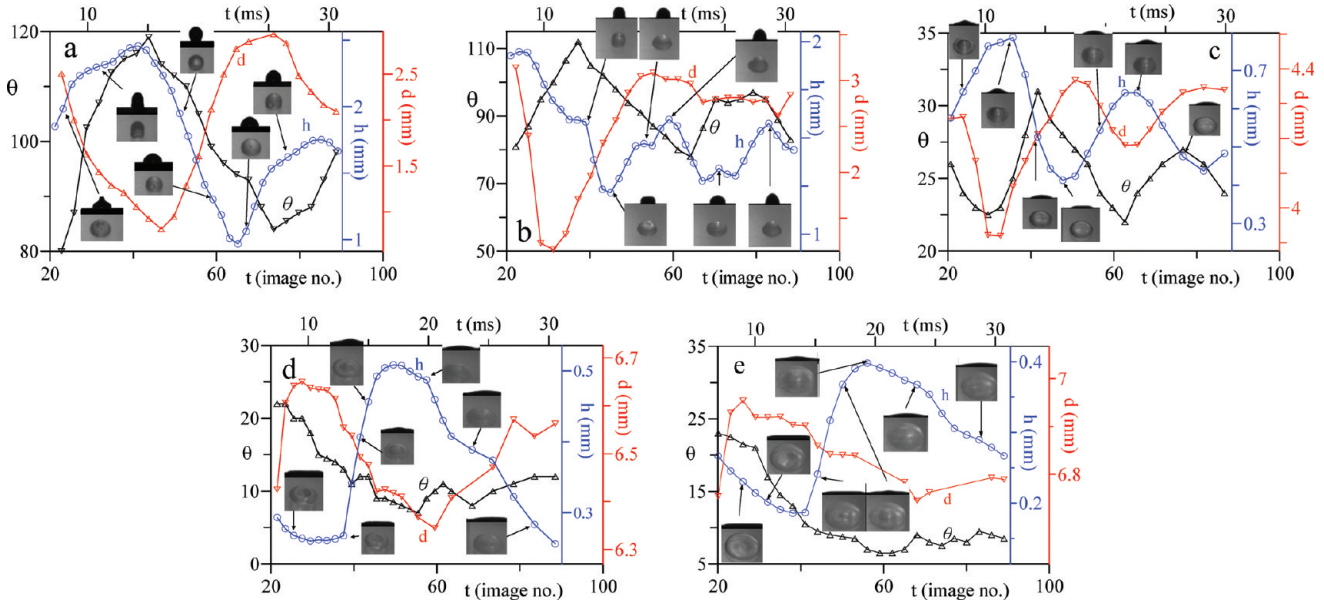

Figure 6. Variation of droplet diameter (d), height (h), and contact angle (θ) for water droplets onto paraffin (a), Teflon (b), glass-2 (c), quartz (d), and clean-glass (e) surfaces, enlarged from Figure 4, showing the relaxation for images 20−90.

much as that on paraffin; the wetting diameter reached its smallest value at 15 pixels. Weaker wetting followed compared with paraffin.

Drop Height. During the intermediate time stage, the oscillation of droplet height depended strongly on the surface hydrophobicity of the substrates. The oscillations of the droplet on clean-glass and quartz were similar: the droplet height decreased in 12 image nos., reached a low height, and stayed around this height for about 25 images, followed by a milder oscillation with a large oscillation period (Figure 4c). Nevertheless, the droplet height recovered in a shorter time for quartz. It is believed that this is because the clean glass has a stronger hydrophilicity.

The oscillation of droplet height for a water droplet on glass-2 was stronger than that on clean-glass and quartz (Figure 4c). Note that the contact angle of a water droplet on glass-2 was higher than for the other two hydrophilic surfaces. The minimum droplet height for droplet on glass-2 was larger than that on clean-glass. In addition, a droplet on glass-2 showed very different height-regaining behavior: (i) the droplet stayed at the minimum height for only a very short period of time, (ii) next, the droplet rose to a higher height than that on clean-glass, and (iii) the oscillation period was shorter for a water droplet on glass-2 (about 40% of clean glass).

Two hydrophobic surfaces demonstrated a very different height oscillation compared with the hydrophilic surfaces. A more significant oscillation of droplet height was observed for the paraffin and Teflon (Figure 4c). Paraffin showed a larger oscillation amplitude than Teflon for the first two cycles, but Teflon had the larger oscillation amplitude from the third cycle. Nevertheless, these two had nearly identical oscillation periods (27 for paraffin and 26 for Teflon), except for the first cycle. It is also interesting to observe that the oscillation on Teflon lasted 1874 image nos., in contrast to 770 image nos. on paraffin, before equilibrium was reached. Figure 7a illustrates the contrast of height oscillation behavior. This difference may due to the different hardness of these two substrates.

The oscillation of droplet height for a water droplet on hydrophobic surfaces lasts many cycles before it disappears (as the amplitude is less than 20 μm). Figure 7a shows that the oscillation amplitude decreased dramatically in the first two cycles

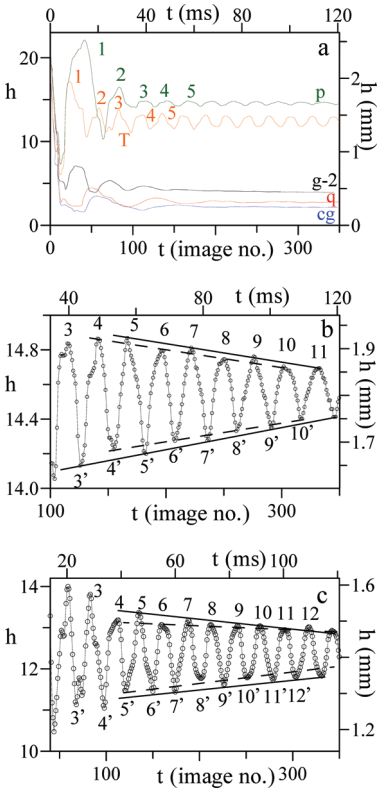

Figure 7. Relaxations of (a) droplet height (h, in pixels) for water droplets impinging onto paraffin (p), Teflon (T), glass-2 (g-2), quartz (q), and clean glass (cg) surfaces and (b, c) the two oscillation modes for odd and even cycles for water droplets on paraffin and Teflon.

for paraffin, but gradually for Teflon. However, the decrease in amplitude was not monotonic. Two oscillation modes on the relaxation of either wave trough or crest can be observed if one carefully examines the data (Figure 7b,c). For the even cycles of oscillation, the wave trough decreased sequentially. However, for the odd cycles, it showed a monotonic decrease. In other words, the *alternative cycles* showed two distinct monotonic decreases.

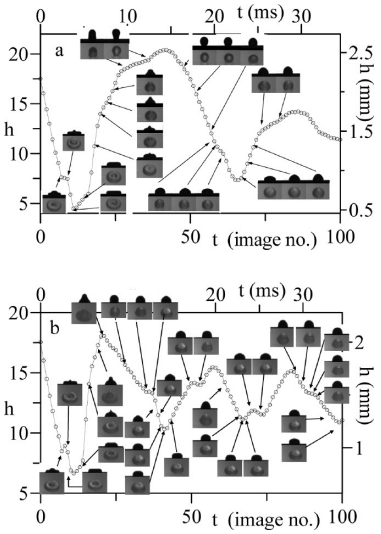

Figure 8. Illustration of droplet images and droplet height (h, in pixels) at various times for water droplets impinging onto paraffin (a) and Teflon (b) surfaces.

Three Modes. More information on the course of the droplet rebound can be obtained if one enlarges the first two oscillation cycles (Figure 8) for the hydrophobic surfaces. The height of the droplet on paraffin increased in three different modes. During images 12−17 (mode A), the growth of the droplet height was mainly due to the increase in the height of the rim because the central conelike region could not be observed from the droplet silhouette. After image 17, the central cone of the droplet appeared on the silhouette again; therefore, the height of the droplet begins increasing dramatically (mode B) due to the fast growth of the small central sharp cone (Figure 8a, images 18−28). On the other hand, during images 29−43 (mode C), the central region merged with the shrinking, upward moving rim into a dull drop where the wetting diameter was equal to or less than the equator diameter. The rate of the increase of droplet height then decreases. Note that the droplet is retracting (d is decreasing) during the above three growth stages (Figure 6a).

For Teflon, similar behaviors were observed (Figure 8b) for modes A (images 12−15) and B (images 26−21). However, the central cone began lowering immediately after mode B, during which time the rim part is retracting and moving upward. Therefore, no mode C was observed.

Further analysis of the motion of the lower and upper parts for the moment immediately following mode B can help detail the differences between paraffin and Teflon. For paraffin, a dull shape where the wetting diameter is equal to or less than the equator diameter was observed in mode C. At this stage, both the upper and lower parts of droplet are moving upward and the droplet height is increasing. For Teflon, the dull shape takes place at images 30−33. At this stage, the lower part is moving upward the upper part is moving downward, and therefore the droplet height is decreasing. No region like mode C for paraffin was observed for Teflon.

For paraffin, the droplet height decreased smoothly after mode C until it reached a minimal height. However, the decreasing course of droplet height showed a complicated behavior for Teflon. After mode B, the central sharp cone descended smoothly. A plateau region was observed during this decreasing course, at image nos. 36−38. Immediately after this plateau, a rapid decrease (image nos. 39−42) was detected. This complicated decreasing course was similar to the plateau found in the first cycle (image nos. 1−12). Both plateau regions corresponded to

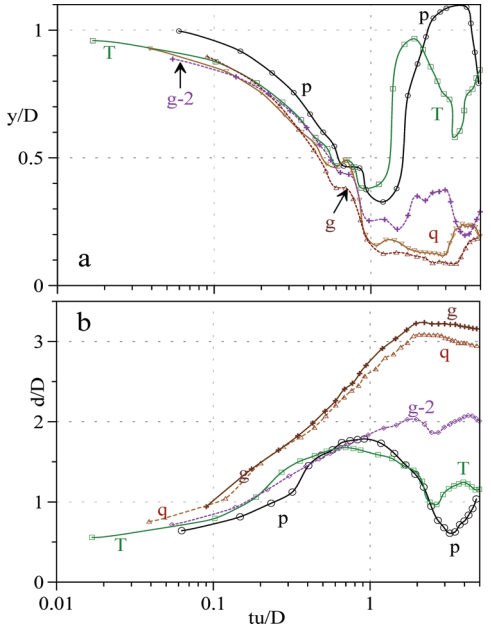

Figure 9. Relaxation of dimensionless droplet height h^* and wetting diameter d^* at initial droplet impact for water droplets released from 13.6 mm above the solid surface of clean glass (g), quartz (q), glass-2 (g-2), Teflon (T), and paraffin (p).

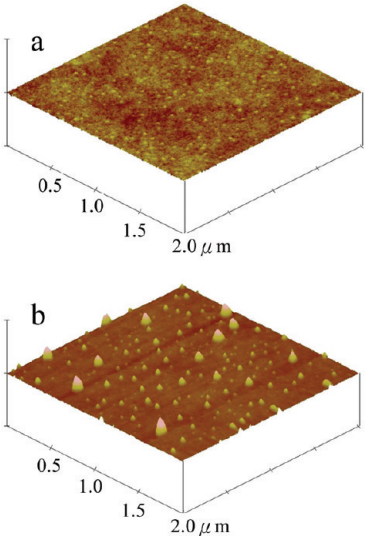

Figure 10. AFM images for substrate surfaces (2 μm × 2 μm) of glass-2 (a) and clean glass (b).

the shape change, from blunt to sharp, of the central upper part of the droplet. Moreover, the next two decreasing courses also exhibited nearly identical behavior (image nos. 59−75 and 85−100).

During the second increasing course, similar three growth modes were observed for paraffin, although the region of mode A was very short. For Teflon, a plateau (with a little bit of overshoot) was seen in the middle of the second increasing course. Note that this second plateau was also due to a shape change from sharp to blunt one for the upper part of the droplet.

Double Rim on Glass. During the first spreading cycle, a clear donutlike (toroid) shape was observed for the paraffin, Teflon, glass-2, and quartz surfaces (Figure 2). It is interesting to note that a water droplet on the glass surface does not form a single donutlike shape. Instead, two toroid rims (one major outside and one minor inside) were observed (image nos. 15−22, column e

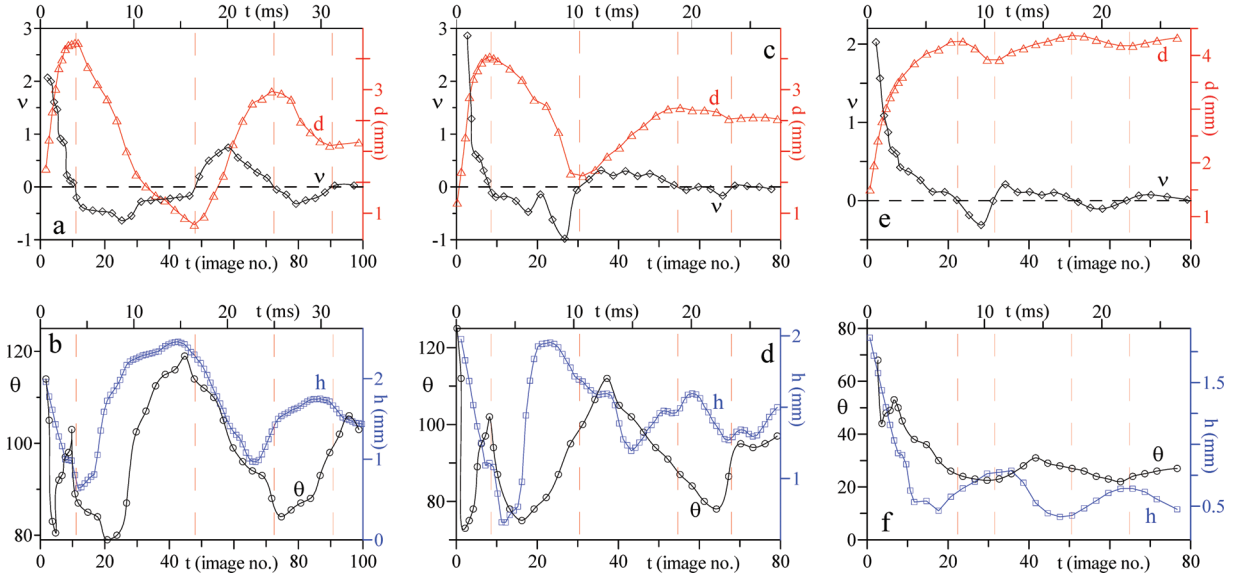

Figure 11. Relaxation of spreading velocity (v, in pixel/image no.), wetting diameter (d), droplet height (h), and contact angle (θ) for water droplets impinging on paraffin (a, b), Teflon (c, d), and glass-2 (e, f).

in Figure 2). This is possibly due to the very fast spreading of the outer part of the droplet on the glass. Because of this, the descending central cone cannot catch up to the outer toroid during its spreading. A second minor toroid rim is therefore formed inside the outer one with the same origin.

Dimensionless Height and Diameter. A notable universal relationship, the dimensionless wetting diameter (d^*) vs dimensionless spreading time (t^*), has been explored for various solid substrates with a wide range of wettability.[5] Furthermore, some literature has reported that the maximum wetting diameter is independent of the hydrophobicity of the substrate.[16]

The relaxations of h and d during early droplet impingement of five different substrates in this work are summarized in Figure 9 using dimensionless parameters. The effect of surface hydrophilicity on the relationship of d^* vs t^* and h^* vs t^* can then be examined.

The data in Figure 9 demonstrate that surface hydrophobicity plays an important role in the dimensionless wetting diameter d^* and droplet height h^*. Moreover, the variance in d^* is more significant than that in h^*. The data also show that quartz and glass have a higher d^* and paraffin has the lowest d^*. It is concluded that a surface with stronger hydrophobicity results in a larger d^*.

Conclusions and Discussion

In this work, the dynamic wetting behaviors of water droplets impinging on five substrates were investigated at fixed Re and We numbers. The images were recorded sequentially, and the full droplet profiles during spreading were summarized and compared to interpret the spreading mechanism. The effects of substrate on the relaxation of the wetting diameter, droplet height, and contact angle were investigated.

The dynamic behaviors of droplet impact were analyzed in detail to study the effects of the substrate. A novel plateau region in the droplet height relaxation profile was observed for all five substrates during the initial spreading. Moreover, on hydrophobic surfaces, the droplet height evolution showed three particular growth modes during each of the ascending and descending courses.

This is the first time that droplet oscillation properties (period, cycle, and oscillation evolution) have been quantified. For hydrophilic substrates, it took only three to five oscillation cycles to reach equilibrium by energy dissipation. A long oscillation period was observed for glass and quartz. For hydrophobic surfaces, 72 and 28 oscillation cycles respectively were required to dissipate the initial kinetic energy for Teflon and paraffin. A much shorter oscillation period (26 and 27, respectively) was observed for these two surfaces. For hydrophobic surfaces, the time required to reach equilibrium was much longer (3−8-fold) than that for hydrophilic surfaces.

It is interesting to note that although Teflon and paraffin present nearly the same hydrophobicity, the droplet oscillation showed distinct rates of energy dissipation for these surfaces. Teflon took 72 cycles (0.65 s), but paraffin took only 28 cycles (0.26 s), to reach the equilibrium state when the water droplet was released from 13.6 mm above the substrate. However, both Teflon and paraffin had nearly the same average oscillation period. We believe that the nearly identical oscillation period was due to the nearly identical surface hydrophobicity. It seems that the greater hardness of Teflon is the cause of the much slower rate of energy dissipation.

For the three hydrophilic surfaces, the time needed to reach equilibrium was nearly the same (image no. 210 ± 10). Nevertheless, the oscillation period of droplet height for a water droplet on clean glass was 2.5 times that on glass-2.

AFM images (Figure 10) showed that the surface roughness of glass increased from 0.27 (glass-2) to 0.42 nm (clean glass washed by cleaning solution for 2 h) in a 2 μm × 2 μm scan area. The increase in roughness may due to the removal of the amorphous region of the top layer and/or the impurities on the surface. The removal of impurities by the cleaning solution was confirmed by the ESCA analyses. The carbon content was found to decrease from 56% (glass-2) to 24% (clean glass), based on the ESCA measurement.

Immediately after droplet impact, the spreading velocity (v) decreased rapidly for all five substrates. The value of v changed from positive to negative in ca. 7 image nos. for hydrophobic surfaces but roughly 23 image nos. for hydrophilic surfaces. It is interesting to note that, for hydrophobic surfaces (Figure 11b,d), (i) the first $v = 0$ (maximum diameter) did not occur at the minimum h, but at the end of the plateau region in the h relaxation course, and (ii) the second $v = 0$ (minimum diameter) did not take

place at the maximum h, but rather during the course of the decreasing h (after the maximum h).

The decreasing h at the second $v = 0$ indicates that the central part of the droplet is moving down when the wetting diameter reaches its minimum value ($v = 0$). The subsequent decrease of h after the maximum wetting diameter at the first $v = 0$ indicates that when the droplet starts to retract from its maximum wetting situation, the central part of the droplet is still moving downward.

Note that the *We* number was fixed (~8) in all experiments presented here. Figure 11b,d indicates that the contact angle (θ) decreases very rapidly during the initial spreading course immediately after droplet impact. This is followed by an increase in θ while the droplet is still spreading, and θ reaches a maximum value at the moment the droplet reaches its maximum diameter.

The rapid decrease in θ indicates there is probably a very thin film near the solid surface running faster than the upper part of the rim region. The subsequent increase of θ implies that the flow in the rim region, driven by surface tension force and kinetic energy, catches up to the thin film spreading at roughly 1 ms (three image nos., Figures 11b,d) later. In other words, the initial, rapid thin film spreading slows down and the upper part of the rim region catches up at the later stage of the wetting, approaching its maximum wetting diameter. The thin film wetting is probably driven by the interfacial interaction between the water droplet and substrate surface.

Similar behavior, a rapid decrease and followed by an increase in θ immediately after the droplet impact, was also observed for a water droplet on the three hydrophilic surfaces, but with a less significant oscillation amplitude. Figure 11f shows a representative θ relaxation for a hydrophilic surface. It is believed that this is a sign that a very thin film wets faster than the upper part of the rim region.

Acknowledgment. The authors express great appreciation to the NSC for the financial support (96-2221-E-011-081).